Polymer Testing 83 (2020) 106374

Contents lists available at ScienceDirect

Polymer Testing

journal homepage: http://www.elsevier.com/locate/polytest

Material Behaviour

Distribution of nanoclay in a new TPV/nanoclay composite prepared through dynamic vulcanization

Sayantani Dutta [a], Srijoni Sengupta [a], Jagannath Chanda [b], Amit Das [b], Sven Wiessner [b], Suprakash Sinha Ray [c], Abhijit Bandyopadhyay [a,*]

[a] Department of Polymer Science & Technology, University of Calcutta, 92, A.P.C. Road, Kolkata, 700009, India
[b] Department of Elastomers, Leibniz Institute for Polymer Research Dresden, Hohe Str. 6, D- 01069, Dresden, Germany
[c] Centre for Nanostructures and Advanced Materials, DSI-CSIR Nanotechnology Innovation Centre, Council for Scientific and Industrial Research, Pretoria 0001, South Africa

ARTICLE INFO

Keywords:
Thermoplastic vulcanizate
Dynamically vulcanized
Organoclay
XRD
DMA
SEM

ABSTRACT

In this article distribution of nanoclay between the two phases of a new class of dynamically vulcanized TPV based on POE/EVA(Polyethylene octene elastomer/ethylene vinyl acetate copolymer) elastomers prepared with various amounts of organoclay (0.5, 1 and 3 wt%) using dicumyl peroxide (DCP) as vulcanizing agent by reactive melt blending process has been studied. Different specimens of POE and POE/EVA blend with and without clay were prepared. The effects of organoclay on mechanical properties, swelling kinetics, crystallinity, vulcanization characteristics, dynamic mechanical behaviour, electrical properties and morphology were studied. DMA and morphological analysis revealed the formation of a Thermoplastic vulcanizate. XRD analysis showed decrease in crystallinity on addition of EVA in POE matrix. However, morphological observation of the fractured surface suggested that the smaller EVA domain was quite uniformly distributed into the POE phase and the clay phase was predominantly dispersed in the EVA phase of the TPVs and 0.5% clay mainly improved the mechanical properties and elongation of the blends. Swelling characteristics, electrical properties and storage modulus were also improved with the clay in case of the blend containing higher EVA content which further supports the fact that nanoclay was preferably distributed in the more polar EVA phase.

1. Introduction

Nanocomposites have drawn much attention in the recent years in many fields of science and technology due to exceptionally high surface area of the reinforcing phase and high aspect ratio which makes them different from other conventional composite materials. The reinforcing materials can be of different forms like particles, sheets or fibers but at least one dimension of these particles must be within 1–100 nm. The extent of enhancement of the properties by these materials depends largely on the dispersion and orientation of the nanofillers in the matrix, interaction of the filler with the matrix, their aspect ratio and also on the mixing/compounding procedure which must be properly controlled. Polymer nanocomposites consist of a polymer or copolymer or even a polymer-polymer blend as matrix to transfer the stress and nanofillers are dispersed uniformly within the matrix to provide sufficient reinforcement. Polymer-layered silicate nanocomposites have attracted lot of interest from both scientific and industrial aspects due to their exceptionally superior mechanical properties [1], improved solvent resistance [2], reduced flammability [3], enhanced ionic conductivity [4] and biodegradability [5] even with minimum clay loading. The first polymer nanocomposite based on nylon 6/layered silicate (MMT) was developed by Toyota Central Research Lab in Japan in collaboration with Ube industries Ltd [1]. Many researchers have afterwards highlighted clay nanocomposites based on various polymers like polypropylene [6], polyethylene [7], polystyrene [8], nylon [9], epoxy resins [10], natural rubber [11], ethylene vinyl acetate copolymer [12], poly(ethylene-co-octene) [13], polyurethane [14], ethylene-propylene-diene monomer (EPDM) [15], Styrene-butadiene rubber (SBR) [16], butadiene rubber acrylonitril -butadiene rubber [17], phenolic resins [18], polyimide [19], poly(methyl methacrylate) [20], polyaniline [21], etc.

Recently another system known as Thermoplastic Vulcanizate (TPV) has become very popular. It is a new class of Thermoplastic Elastomer (TPE) which consists of a rubber/plastic polymer mixture in which the

* Corresponding author.
E-mail address: abpoly@caluniv.ac.in (A. Bandyopadhyay).

https://doi.org/10.1016/j.polymertesting.2020.106374
Received 19 September 2019; Received in revised form 16 January 2020; Accepted 21 January 2020
Available online 24 January 2020

rubber phase is predominantly vulcanized during processing by the use of an appropriate curative when mixed with a thermoplastic polymer. The main feature of this class of polymers which makes them different from others is that they can be melt processed and also can perform like conventional vulcanized rubber. Dynamic vulcanization improves the performance of the TPV. Presently TPVs have so many advantageous properties like good gloss, recyclability, improved colorability, shorter cycle time, design flexibility, low cost, low density and excellent wear ability, etc. for which they have been recently replacing EPDM rubber in various applications. TPVs are opening new fields of applications as automotive parts, footwears, packaging, cable insulation, medical devices, etc [22,23]. Dynamic vulcanization technique was first introduced by Gessler and Haslett for the preparation of iPP/Polyisobutylene blend [24]. The first TPV commercialized in the market was introduced by Fischer consisting of EPDM/PP in which the EPDM phase was partially crosslinked [25]. Later on Coran, and Patel developed TPVs consisting of fully vulcanized rubber in the plastic phase [26].

In this article we have reported the preparation and characterization of a TPV/Organoclay nanocomposite based on POE/EVA blend and showed the distribution of the clay between the different phases. Various TPVs and also TPV/Organoclay nanocomposites have been developed in the last few years [27–31] but probably no research has been reported on the POE/EVA/organoclay based thermoplastic vulcanizate nanocomposite as well as about the distribution of the nanoclay in the TPV so far. H.H. Le et al. showed a very good dispersion of the nanofillers in different rubber matrix by using dispersing agents like carboxylated NBR, ionic liquid and ethanol [32]. Poly (ethylene-co-octene) elastomer commercially named as Engage^{R} has been developed using metallocene catalyst. It is a new class of elastomer which has received much attention due to its uniform distribution of comonomer content, narrow molecular weight distribution, controlled long chain branching, good electrical and thermal properties, improved flex fatigue resistance, easy processability, unique mechanical and rheological properties, etc. Depending on the octene content different grades are available. They find extensive application in cable industry, footwear, foams, pipes, rotomolded articles and also in automotive industry. Various modifications on the matrix of Engage^{R} have been reported so far [33–35]. Ethylene vinyl acetate (EVA) copolymers are available as rubber, plastics and also thermoplastic elastomer depending on the vinyl acetate content. This class of copolymer provides quite better mechanical and thermal properties to the finished products due to their high molecular weight. They find widespread application in the field of wire and cable industry, footwear, packaging, adhesive, sealants etc. Engage^{R}-EVA blends are quite popular in footwear, cable and foam industry. Naskar, Mohanty and Nando [36] reported the application of dicumyl peroxide/triallyl cyanurate cured Engage^{R}-EVA blend for the development of the thin-walled halogen free cable insulation and thin-walled halogen free fire resistant low smoke cable sheathing. Modification of Engage^{R} or POE with high vinyl acetate content EVA was reported by Pervin et al. [37] Horng-jer Tai reported random crosslinking between POE and EVA in presence of triallyl cyanurate by reactive blending [38].

In the present work Engage 8440, DuPont Elvax 40L-03 and Montmorillonite (MMT) clay were taken for the preparation of the TPV/Organoclay nanocomposite. Montmorillonite (MMT) is the most commonly used layered silicate clay which consists of an octahedral alumina sheet sandwiched between two tetrahedral silica sheet. Sodium montmorillonite (NaMMT) is a hydrophilic material. Organic modification of NaMMT is accomplished by introducing a long alkyl chain in the clay gallery via the cation exchange process to make it hydrophobic in nature as well as to increase its compatibility with organic polymers. Several modification systems are available based on quaternary ammonium surfactant, alkyl imidazoles and phosphorous ionic compounds. For this work 25–30 wt % methyl dihydroxyethyl hydrogenated tallow ammonium modified montmorillonite was used as the reinforcing agent. The chemical structure of the organic modifier is shown below

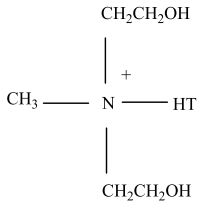

Scheme 1. Chemical structure of tallow amine used a modifier of Na-MMT.

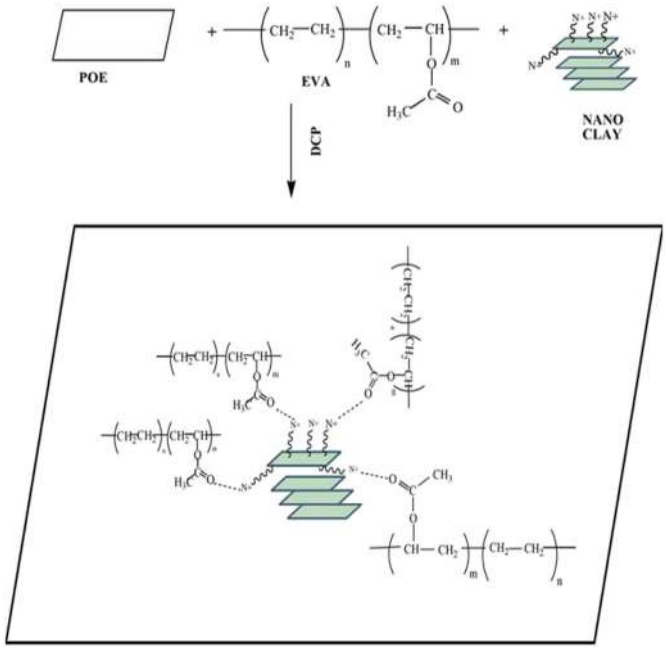

Scheme 2. Probable mechanism of interaction of nanoclay with EVA matrix.

(Scheme 1) and the interaction of the clay with the EVA phase of the TPV is shown in Scheme 2. The nanocomposites were prepared by reactive melt blending process in a Brabender Plastograph instrument.

2. Experimental

2.1. Materials

The base elastomer used in this experiment was Poly(ethylene-co-1-octene) (POE) of trade name ENGAGE^{R} 8440 of density 0.897 g/cc, MFI 1.6, total crystallinity 27%, hardness 86 (Shore A), glass transition temperature −33 °C and melting temperature 93 °C was purchased from Dow Chemical's (Switzerland). Poly(ethylene-co-vinyl acetate) (Elvax 40L-03) of 40% vinyl acetate content, density 0.967 g/cc, MFI 3, glass transition temperature −37 °C, melting temperature 58 °C, along with low gel content, high molecular weight and high polarity was supplied by DuPont. The organic peroxide used as vulcanizing agent was dicumyl peroxide (DCP with 99% purity), was procured from Aldrich Chemicals. Coagent (Aurosin 6860), an acrylate based multifunctional organic compound was gifted from Auropol India Pvt. Ltd and was used with DCP to increase the crosslinking efficiency. The nanoclay used for reinforcement was 25–30 wt % methyl dihydroxyethyl hydrogenated tallow ammonium modified montmorrilonite, was procured from Aldrich Chemicals. Toluene with 99% purity, water content less than 0.1%, was used as the solvent for the swelling study and was purchased from Merck specialities Pvt. Ltd. Acetone with purity 99.5% and water content less than 0.2%, also used for washing the mold and the mold

Table 1
Composition of the samples.

Sample Notation	POE Content (grams)	EVA Content (grams)	Organoclay content (wt%)	DCP content (wt%)	Coagent Content (wt%)
E_0	44	0	0	1	1
E_{90}	39.6	4.4	0	1	1
E_{80}	35.2	8.8	0	1	1
E_{60}	26.4	17.6	0	1	1
$E_{0/N0.5}$	44	0	0.5	1	1
$E_{0/N1}$	44	0	1	1	1
$E_{0/N3}$	44	0	3	1	1
$E_{90/N0.5}$	39.6	4.4	0.5	1	1
$E_{90/N1}$	39.6	4.4	1	1	1
$E_{90/N3}$	39.6	4.4	3	1	1
$E_{80/N0.5}$	35.2	8.8	0.5	1	1
$E_{80/N1}$	35.2	8.8	1	1	1
$E_{80/N3}$	35.2	8.8	3	1	1
$E_{60/N0.5}$	26.4	17.6	0.5	1	1
$E_{60/N1}$	26.4	17.6	1	1	1
$E_{60/N3}$	26.4	17.6	3	1	1

plates was supplied by Merck specialties Pvt. Ltd.

2.2. Preparation of POE/EVA blend

Thermoplastic vulcanizates were prepared by dynamic vulcanization in Brabender Plastograph (made in Germany TYP 815606) at proposed temperatures and 60 rpm speed. EVA was first separately mixed with 1% DCP and coagent (1% with respect to the DCP) for 2 min at 120 °C and then taken out from the mixer and cut into small pieces. POE was then preheated with 1% DCP and coagent (1% with respect to the DCP) for 1 min at 180 °C; melted EVA pieces were then added to this mixture at the same temperature and mixed for further 4 min. The final batch weight was 44 g. The mixture were taken outside, cut into small pieces with a knife and cooled. Finally, about 40 gm of the blend pellets were taken and compression molded in a hydraulic press at 180 °C under 15 ton pressures for 5 min. The pressure was then released after room temperature was attained.

2.3. Preparation of POE/EVA/Organoclay nanocomposite

Nanocomposites of different batches of the TPVs were also prepared by mixing in the same Brabender Plastograph. Here again the EVA was premixed with 1% DCP and coagent (1% with respect to the DCP) for 2 min and then taken out from the mixer and cut into small pieces. POE was then preheated with 1% DCP and coagent (1% with respect to the DCP) for 1 min at 180 °C, and then melted EVA pieces were added to this mixture at the same temperature and mixed for further 2 min. Finally, the clay was added and mixed for another 2min. The final batch weight was 44 g. The mixture were taken outside, cut into small pieces with a knife and cooled. Finally, about 40 gm of the blend pellets were taken and compression molded in the hydraulic press at 180 °C under 15 ton pressure for 5 min. The pressure was released after room temperature was attained. Compositions of all the batches are shown in Table 1.

2.4. Characterization

Vulcanization Characteristics: Vulcanization Characteristics of the samples were studied using Brabender Plastograph made in Germany TYP 815606 at 180 °C and a rotor speed of 60 rpm. The change in the torque with time during mixing was recorded from the software attached with the Brabender.

Infrared Spectroscopic Analysis: Fourier Transform Infrared (FTIR) spectroscopic analysis of the samples with and without clay were accomplished in ALPHA E Bruker, Germany spectrophotometer. The samples were characterized directly in sheet form in ATR mode within a spectral range of 500–4000 cm^{-1}. The crystal used for ATR configuration was made up of zinc selenide.

2.4.1. Mechanical properties

Tensile properties: Mechanical properties including tensile strength, tensile modulus (300%), total elongation at break were measured using the UTM LLOYD instrument (LR 10 K plus, Load Cell 10 KN) at a strain rate of 500 mm/min. All the measurements were performed at room temperature until the specimen ruptured. Dumbbell-shaped specimens were punched out from the sheets under investigation using a die constructed in accordance to ASTM D412. Three specimens for each compositions were tested and values were reported, obtained from the software attached with the machine.

Hardness: In this investigation hardness was measured by Durometer Shore A tester, at room temperature. Each sample was tested for three times and the average result was reported.

X-ray Diffraction Analysis: X-ray diffraction studies of the samples were carried out using X'pert PRO MRD X-ray diffractometer (PANalytical, The Netherlands) in the range of $2\theta = 3$–$50°$ using CuKα radiation ($\lambda = 0.154$ nm) at acceleration voltages of 40 kV and beam current of 30 mA.

Percentage of crystallinity was determined using eq. (2).

$$\% \text{ of Crystallinity} = [A_c/(A_c + A_a)] \times 100 \quad (2)$$

A_c represents the area of the crystalline phase, A_a represents the area of the amorphous phase and $(A_c + A_a)$ represents the total area.

The crystallite thickness was calculated using the Scherrer equation (eq. (3)).

$$\tau = k\,\lambda / \beta \cos\theta \quad (3)$$

Where, τ is the crystallite thickness, k is the shape factor with a typical value of 0.9 but varies with the actual shape of the crystallite, λ is the wavelength of X-ray, β is referred to as full width at half the maximum intensity (FWHM) and θ is the Bragg's angle.

Again, the interplanner distances were calculated using Bragg's Law which is,

$$n\,\lambda = 2d_{001}\sin\theta \quad (4)$$

Where n is an integer for only constructive interferences, d_{001} is the interplanner distance (reflection occurs from the [001] plane here), λ and θ are of same meaning as mentioned above.

The number of clay platelets per average stack with the interplanner distance d_{001} was calculated using the following formula [39].

$$N = 1 + \tau / d_{001} \quad (5)$$

Scanning Electron Microscopy: All SEM images of the fractured surfaces were acquired on a NEON 40 EsBs Cross beam scanning electron microscope from Carl Zeiss NTS GmbH, operating at 3 kV in the secondary electron (SE) mode. To enhance electron density contrast, each sample was coated with platinum (3.5 nm) using a Leica EM SCD 500 sputter coater.

Dynamic Mechanical Analysis: Dynamic mechanical properties were studied using a dynamic mechanical analyzer (DMA) instrument (METRAVIB VA4000) at a frequency of 11 Hz, heating rate of 5 °C/min, 0.1% strain and temperature range 30 °C–150 °C in a tension-compression model and the data were recorded from the software attached with the machine. Storage modulus (E′), loss modulus (E″) and loss tangent (tan δ) were measured as a function of temperature for all the samples under identical conditions. In this investigation the temperatures corresponding to the peaks in the tan δ versus temperature plot were taken as the softening temperatures.

Swelling Behavior: Samples with definite shapes and uniform dimensions were cut from the sheets, gently wiped to remove the dust, weighed in a digital balance and then immersed in a particular amount

Table 2
Maximum Torque, 300% Modulus, Hardness, and Crystallinity of POE, POE/EVA blends and its nanocomposites.

Sample	Max Torque (Nm)	Time (sec)	Tensile Modulus (300%) (MPa)	Tensile Strength (MPa)	Elongation at break (%)	Hardness (Shore A)	Bragg's Angle	d_{001}	% Crystal-linity	FWHM	Crysta-llite thickness (A°)	N
E_0	16	120	8.86	14.83	718.51	85	21.05	4.22	21.32	0.1624	8.68	–
E_{90}	15.9	116	8.7	12.86	626.52	84	21.54	4.12	18.65	0.1624	8.69	–
E_{80}	12	115	7.6	11.05	613.59	75	21.49	4.13	16.88	0.3247	4.34	–
E_{60}	11.5	110	6.56	9.84	640.92	70	21.68	4.09	14.22	0.396	3.56	–
$E_{0/N0.5}$	15.7	108	5.85	10.17	397.86	88	21.55	4.12	17.006	0.3897	3.62	1.9
$E_{0/N1}$	16	100	8.12	11.64	607.17	81	21.54	4.12	17.79	0.4546	3.10	1.75
$E_{0/N3}$	17.1	98	9.15	12.82	560.87	80	21.58	4.11	17.99	0.2273	6.21	2.51
$E_{90/N0.5}$	18.8	126	9.28	15.46	724.897	87	21.66	4.09	23.68	0.13	10.85	3.65
$E_{90/N1}$	12	118	7.24	9.423	427.7	81	21.59	4.11	15.63	0.4221	3.34	1.81
$E_{90/N3}$	14.4	118	8.69	11.67	571.05	86	21.61	4.11	16.03	0.2922	4.83	2.18
$E_{80/N0.5}$	13	170	7.82	11.57	651.13	85	21.53	4.12	17.001	0.3297	4.34	2.05
$E_{80/N1}$	15.9	116	7.53	8.98	443.586	82	21.58	4.11	15.29	0.3572	3.95	1.96
$E_{80/N3}$	8.7	144	6.785	8.859	545.98	80	21.54	4.12	12.36	0.4546	3.10	1.75
$E_{60/N0.5}$	15	130	7.04	9.69	545.79	80	21.58	4.11	15.22	0.1948	7.24	2.76
$E_{60/N1}$	13.6	122	6.5	5.73	241.43	75	21.64	4.10	14.41	0.3247	4.35	2.06
$E_{60/N3}$	14.2	124	7.28	9.21	504.43	80	21.61	4.11	14.69	0.2922	4.83	2.175

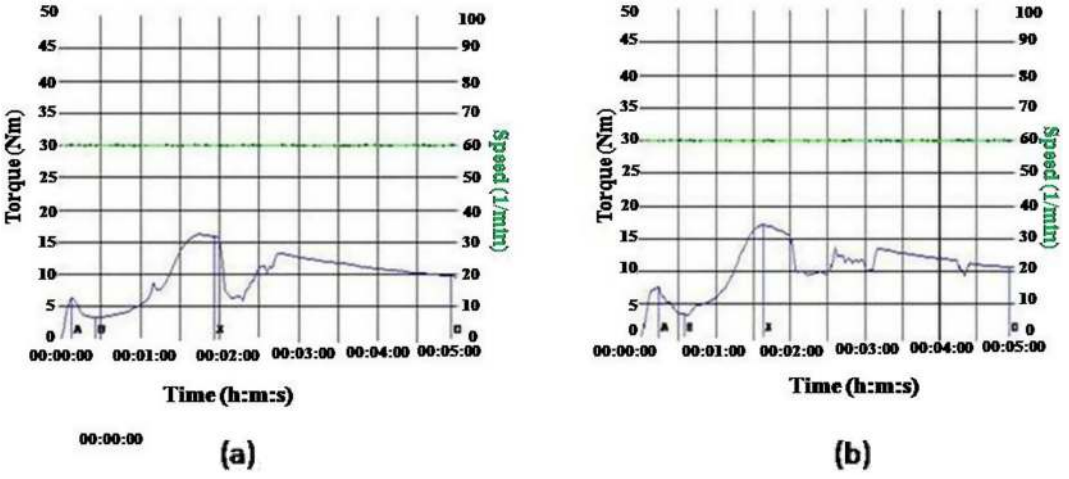

Fig. 1. Mixing torque-time profile for (a) E90 and (b) E90/N0.5.

of toluene at room temperature. After fixed time intervals the samples were taken out from the solvent, carefully wiped out with a tissue paper to remove the toluene adhered on the surface of the sample and weighed in the same digital balance to determine the amount of solvent absorbed. This process was continued till equilibrium swelling was reached which was indicated by the constancy in weight of the material. Each weighing was completed within very few seconds to avoid any error due to solvent escape. Swelling ratio was calculated using eq. (1).

$$\text{Swelling ratio} = (W_f / W_i) \ldots\ldots\ldots\ldots\ldots\ldots\ldots\ldots\ldots\ldots \quad (1)$$

W_f denotes the weight of the samples after absorption of the solvent and W_i denotes the initial weight of the sample. Swelling ratio values were plotted against time to compare the solvent resistivity of the samples.

AC Resistivity Analysis: The AC resistivity of the samples was measured using Dielectric Breakdown Voltage Tester model S-1133 of output voltage 0-60 KV. Samples were cut into small pieces from the compression molded sheets to fit between the electrodes and breakdown voltage was determined very carefully.

3. Result and discussion

3.1. Studies on mixing torque

Table 2 shows the correlation between the mixing torque and the 300% modulus of POE-EVA blend and POE/EVA/nanoclay composites during the mixing time. Torque is the resistance offered by the material during mixing.

There is a linear relationship between the mixing torque and the melt viscosity of all the batches under investigation. High torque value implies higher viscosity of the sample which is usually directly proportional to its tensile modulus and higher the tensile modulus value higher is the strength of the specimen. In this experiment, $E_{90/N0.5}$ shows the highest torque as well as the highest tensile modulus value (Fig. 1). Upon addition of clay approximately all the batches showed an increase in torque as well as in tensile modulus. The maximum torque was obtained after 2 min during mixing which means after the addition of EVA and elucidates the formation of a TPV during mixing.

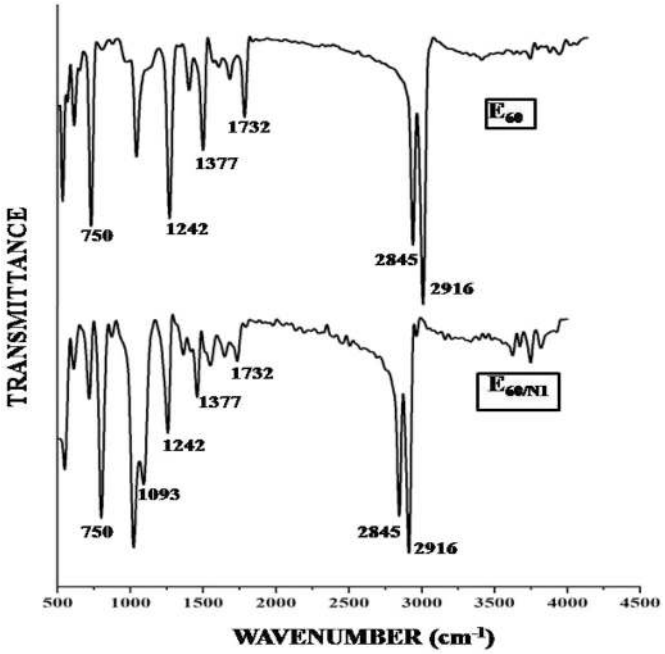

Fig. 2. FTIR spectra of E60 and E60/N1.

3.2. Spectroscopic analysis

The FTIR spectra of the sample with and without clay are shown in Fig. 2. The spectrum shows the following characteristic peaks: at 750 cm-1 for pendant octane unit of POE in both E60 and E60/N1, ~2910 cm-1 for C–H asymmetric stretching vibration of CH2 and ~2845 cm-1 for C–H symmetric stretching of the CH2 respectively, at 1732 cm-1 for C═O stretching vibration for EVA, at 1377.97 cm-1 and 1242 cm-1 for C–O stretching vibration of ester and at 1093.93 cm-1 for stretching vibration of Si–O due to the presence of clay in E60/N.

The peak at 1732 cm-1 (C═O) for EVA in E60 did not shift in E60/N1 meant that, the clay did not produce any strong chemical interaction with the matrix thus the interaction is stated to be a physical one.

3.3. Studies on mechanical, dynamic mechanical, morphological and electrical properties of POE/EVA TPVs and their nanocomposites

All mechanical properties are reported in Table 2. It was found that the tensile strength, elongation at break, tensile modulus (300%) and the hardness of neat POE were 14.83 MPa, 718.51%, 8.86 MPa and 85 Shore A respectively. Addition of EVA in POE decreased all the above said properties. This can be explained on the basis of decrease in crystallinity of POE upon addition of EVA which can be further supported by the X-ray diffractograms demonstrated in Fig. 6. With increase in EVA content all those properties were found to be decreased in the following manner $E_0 > E_{90} > E_{80} > E_{60}$. Addition of 0.5 wt% clay increased the tensile strength, net elongation tensile modulus and hardness up to 15.46 MPa, 724.897%, 9.28 MPa and 87 Shore A respectively for E_{90} and

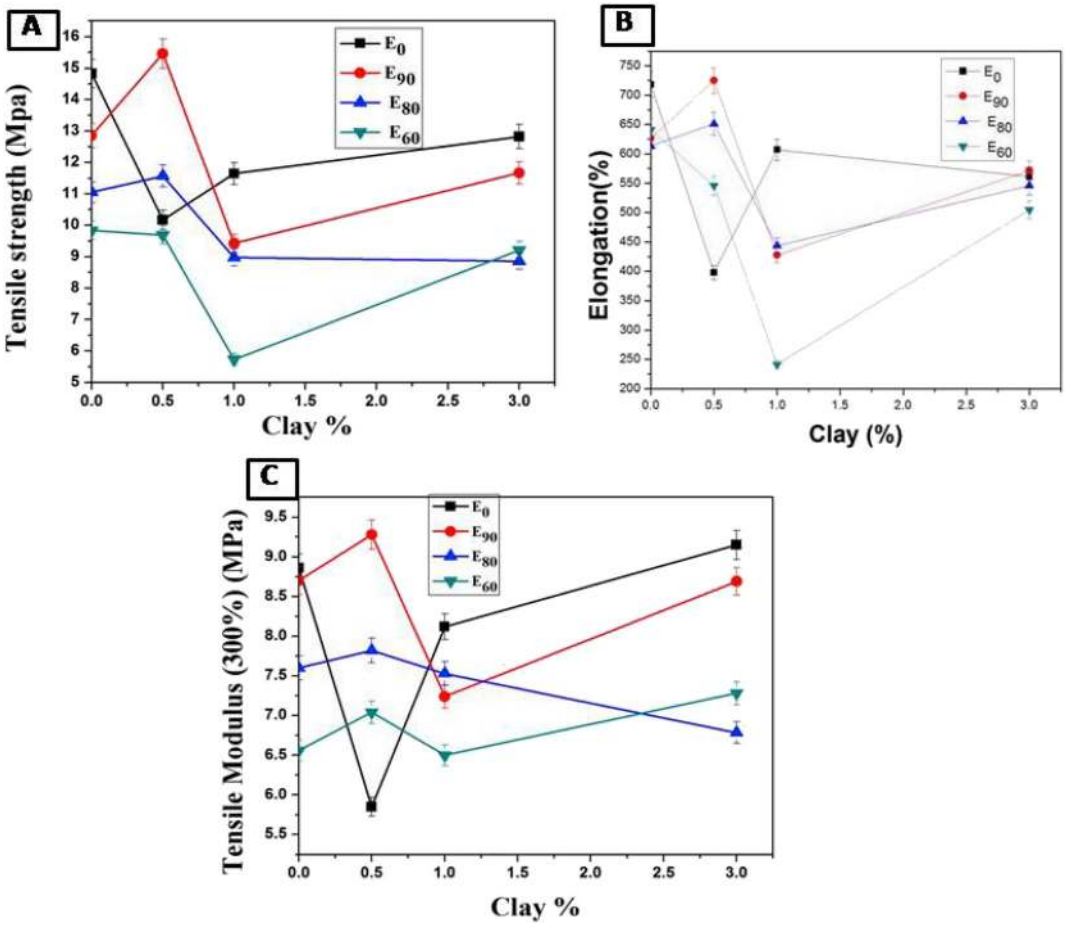

Fig. 3. Summary of mechanical properties with loading percent of clay (A) Tensile strength, (B) Elongation, (C) Tensile Modulus (300%).

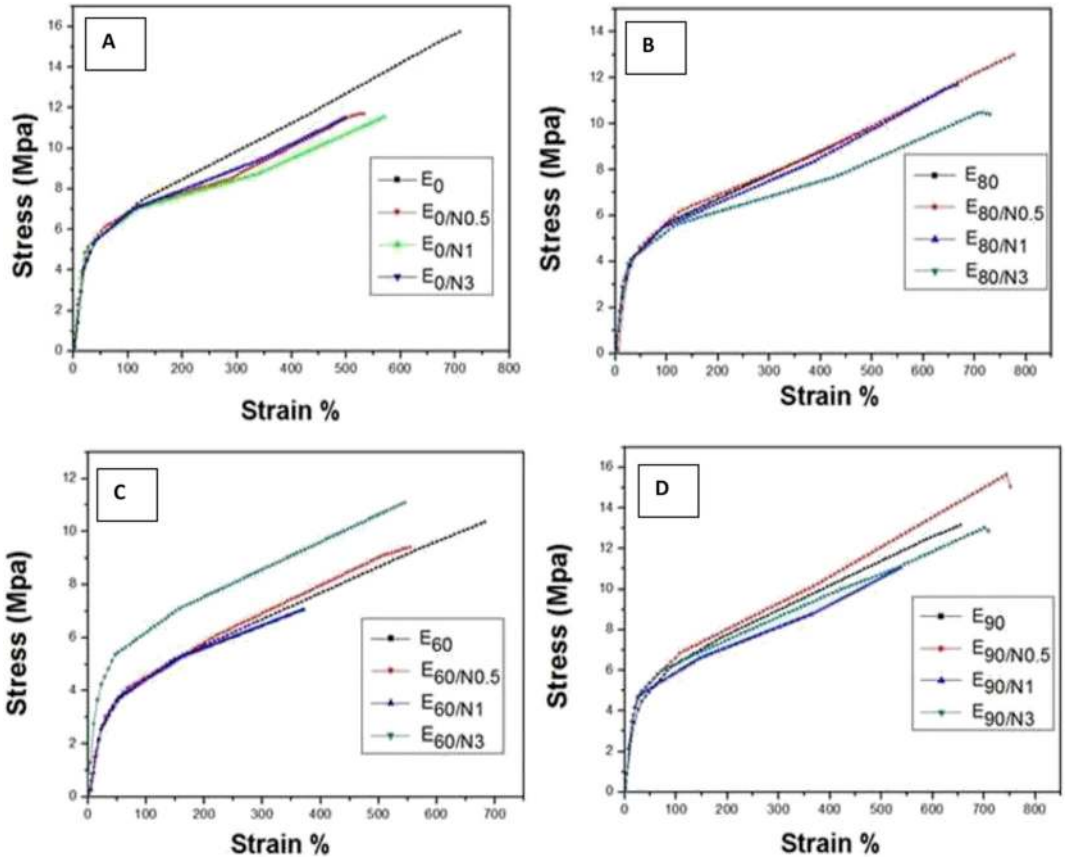

Fig. 4. Tensile stress–Strain plot of (A) POE with its different composition of clay, (B) POE/EVA (80:20) with its different composition of clay, (C) POE/EVA (60:40) with its different composition of clay, (D) POE/EVA (90:10) with its different composition of clay.

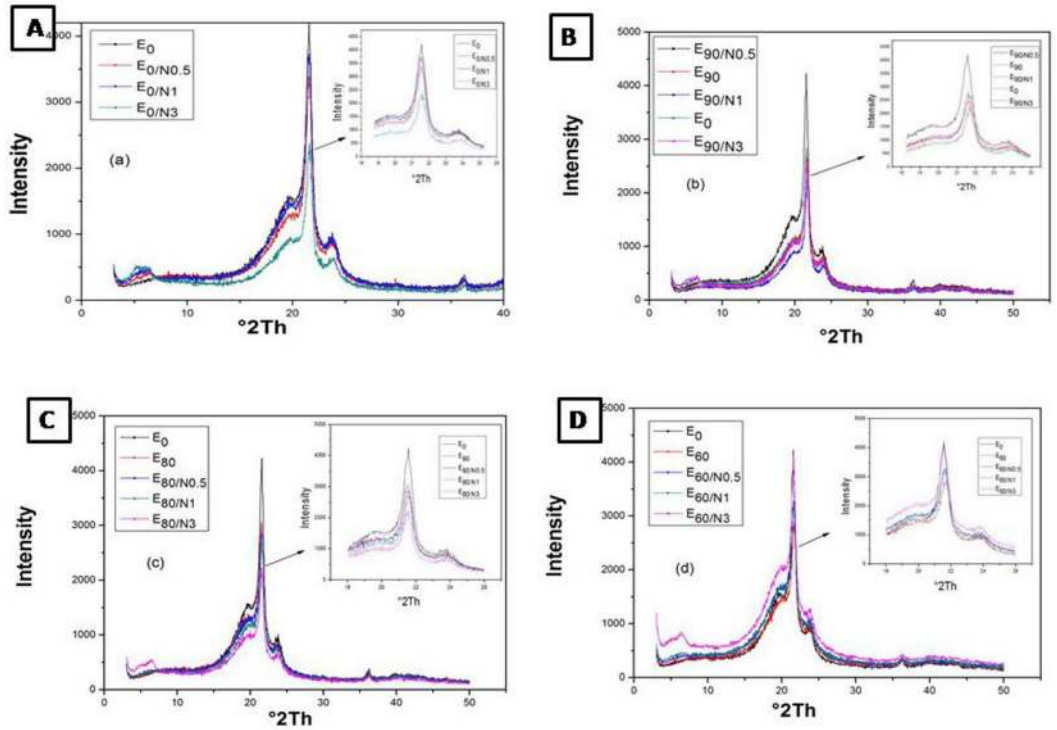

Fig. 5. XRD Spectrum of different composites of clay with (A) POE, (B) POE/EVA (90:10) blend, (C) POE/EVA (80:20) blend and (D) POE/EVA (60:40) blend.

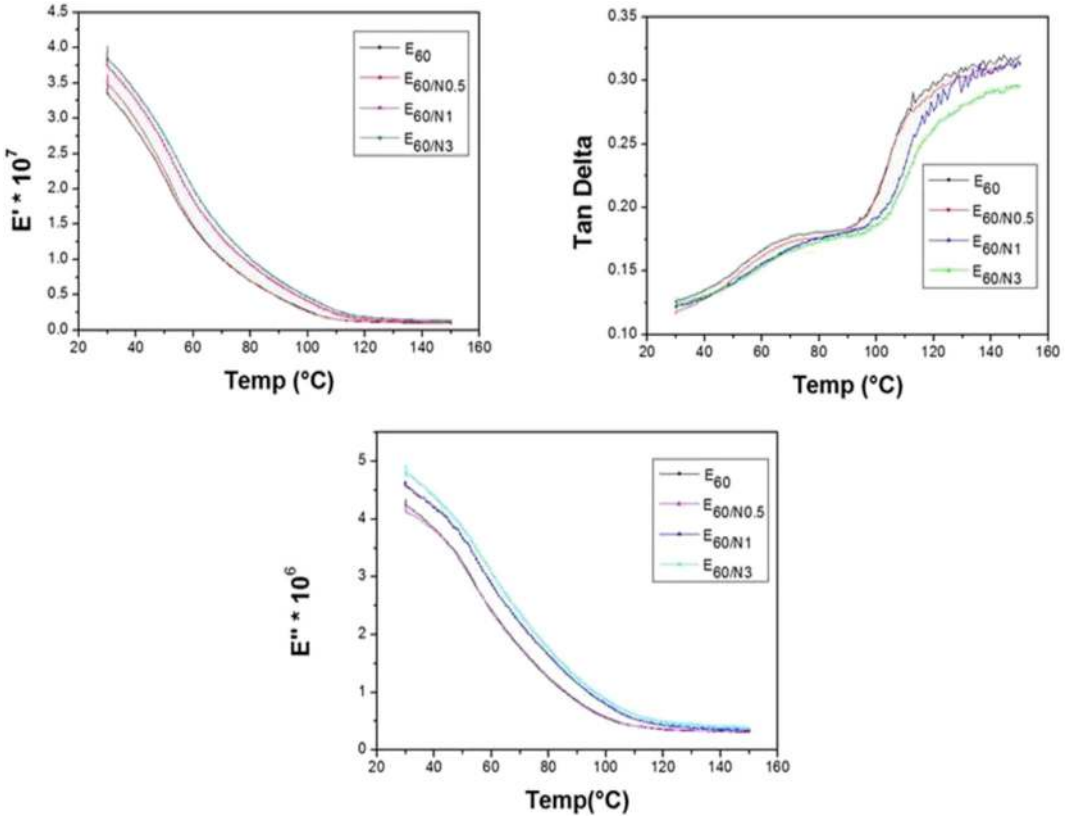

Fig. 6. DMA results of POE/EVA (60:40) blend and its different composites with clay.

11.57 MPa, 651.13%, 7.82 MPa and 85 Shore A respectively for E_{80}. But addition of clay did not improve the tensile strength and net elongation in cases of E_0 and E_{60}. 300% Modulus decreased from E_0 to $E_{0/N0.5}$ and further increased in $E_{0/N1}$ to $E_{0/N3}$. This deviation can be attributed towards the poor dispersion of the clay in the POE/EVA matrix, stress accumulation and also due to drop in crystallinity as demonstrated in Fig. 5.

Tensile strength and net elongation profiles of all the batches are

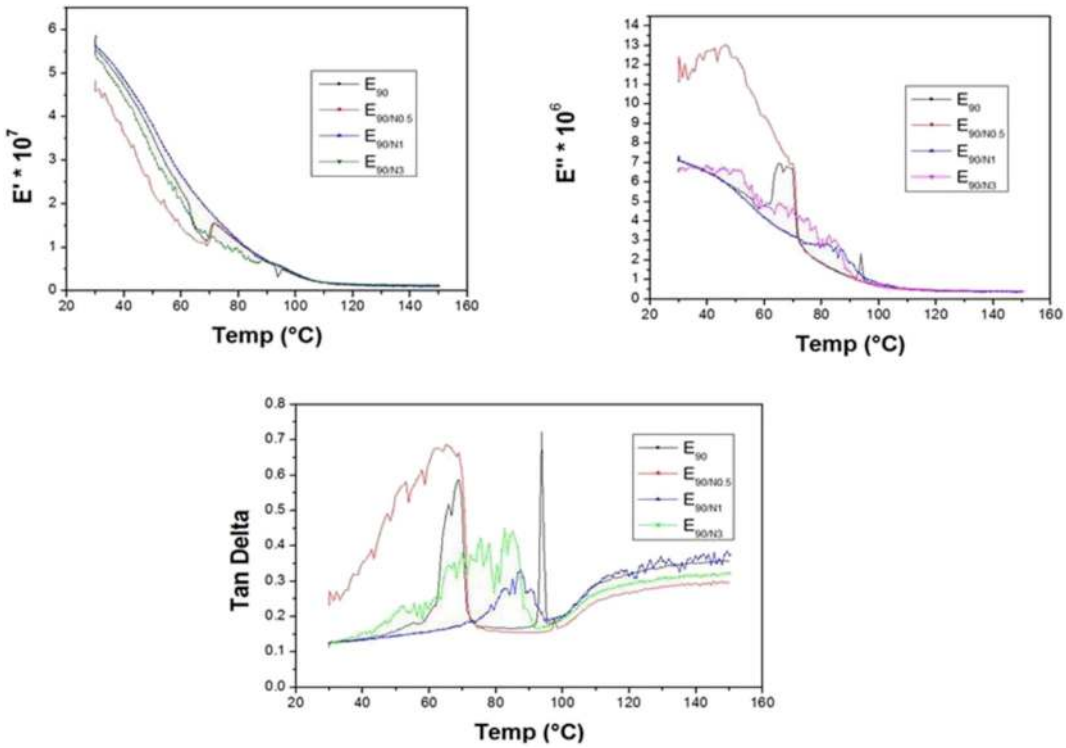

Fig. 7. DMA results of POE/EVA (90:10) blend and its different composites with clay.

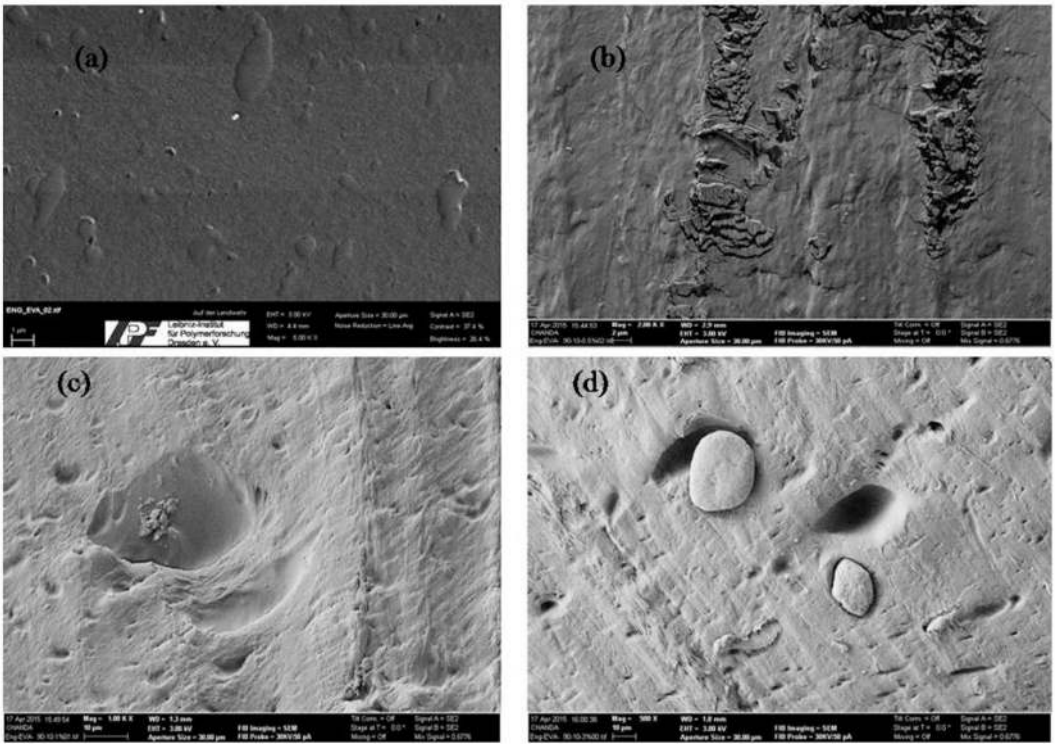

Fig. 8. SEM images of (a) E_{90}, (b) $E_{90/N0.5}$, (c) $E_{90/N1}$, (d) $E_{90/N3}$.

delineated in Fig. 3.

Tensile modulus and hardness values, however, increased upon addition of 0.5 wt% clay in all the batches under investigation due to better interfacial interaction (physical) between the clay and POE/EVA matrix which can be further confirmed from the morphology analysis. Tensile modulus behavior is demonstrated in Fig. 3. 1 wt% and 3 wt% clay could not significantly improve the mechanical properties due to poor dispersion of the clay.

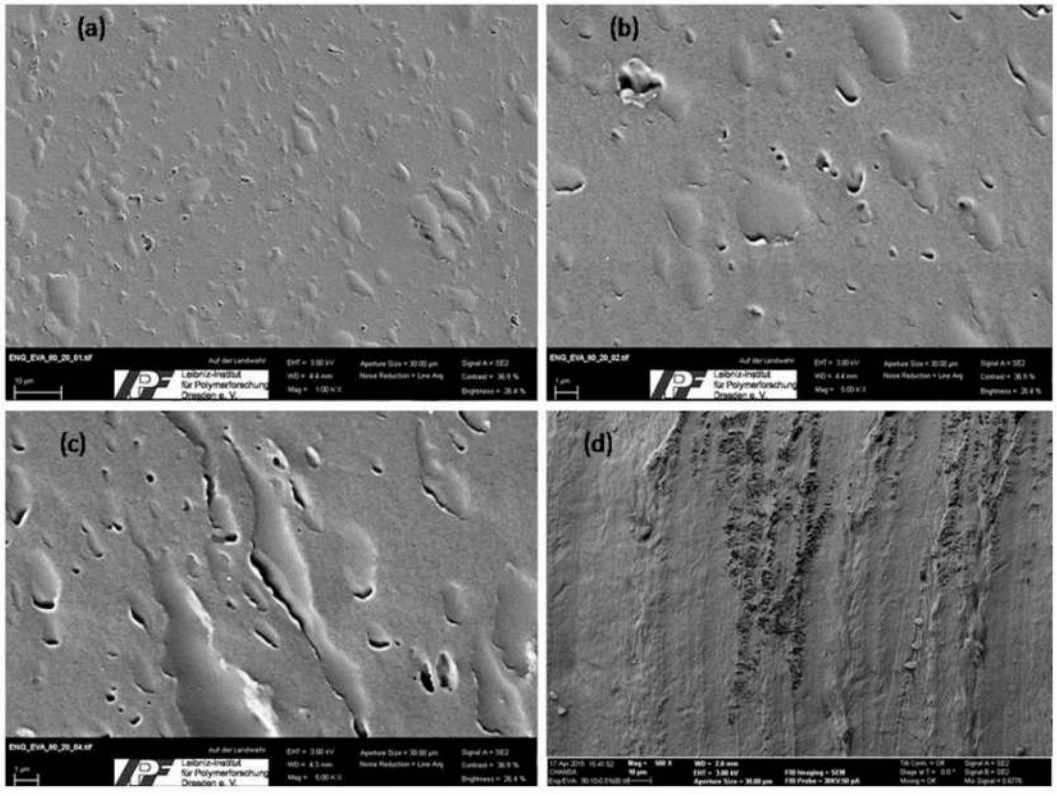

Fig. 9. SEM images of (a) E_{80}, (b) $E_{80/N0.5}$, (c) $E_{80/N1}$, (d) $E_{80/N3}$.

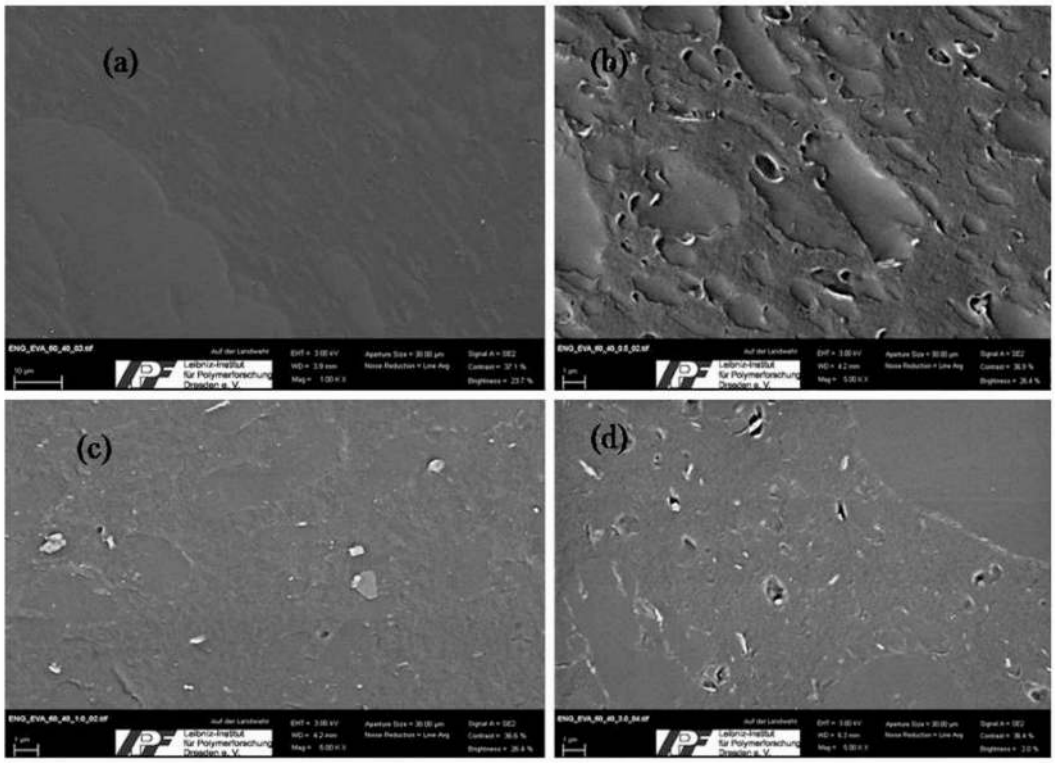

Fig. 10. SEM images of (a) E_{60}, (b) $E_{60/N0.5}$, (c) $E_{60/N1}$, (d) $E_{60/N3}$.

Tensile stress-strain profiles are shown in Fig. 4 which is in good agreement with the theoretical reasons.

The wide angle X-ray diffractograms are shown in Fig. 5. Diffractogram of POE exhibited one major peak located at 21.058°. The net crystallinity and the crystallite thickness are calculated and reported in Table 2. Upon addition of clay the peak position remained fixed but the intensity of the peak dropped which means there was a fall in crystallinity in POE. The fact that the degree of crystallinity largely depends on the clay content as it acts as barrier against the crystal growth. As a consequence of this $E_{0/N0.5}$, $E_{0/N1}$ and $E_{0/N3}$ shows lower degree of crystallinity and crystallite thickness than that of E_0, which is also supported by the peak broadening of the corresponding POE-clay nanocomposites and their mechanical properties showed similar trend. Similarly in E_{90} grade, the hardness varied along with the crystallinity. Again it was noticeable that addition of EVA on POE also decreased the degree of crystallinity which is supposed to be due to the lower crystallinity of the EVA component. The diffractograms of the POE/EVA blends also showed one major peak near the same range as in case of POE which suggests that the peak of the EVA component is superimposed on the peak of POE as it also exhibits a peak between the same range. It was observed that addition of 0.5% clay increased the degree of crystallinity as well as other mechanical properties of E_{90} and E_{80} significantly.

In case of E_{60} addition of 0.5% clay though slightly increased the degree of crystallinity and modulus but no such significant rise in the strength and net elongation were seen. Poor tensile strength might be due to the poor dispersion of the clay on POE matrix as EVA component constitutes a large portion in this batch which is of lower strength than POE. The reason behind the decrease in net elongation was supposed to be due to the poor stress transfer characteristics of the matrix.

The values of FWHM and crystallite thickness are in good agreement with the theoretical explanation of the degree of crystallinity trend. Fig. 6 and Fig. 7 demonstrate the DMA diagrams of POE/EVA (60:40) and POE/EVA (90:10) batches. For both the batches tan δ versus temperature plot shows two characteristic peaks at the melting temperature (T_m) of EVA of around 60 °C and melting temperature (T_m) of POE of around 100 °C which clearly corresponds to the phase separation of the two components.

It is evident from Fig. 6 that both the storage modulus and loss modulus were increased with gradual increase in the clay content suggesting good mechanical reinforcement inspite of lower tensile strength. It may be due to the fact that clay phase had stiffened the matrix and simultaneously the viscous content was also increased. Peak height of the tan δ versus temperature also decreases gradually from 0% to 3% clay. It may correspond to the fact that cooperative movement of the molecules becomes greater suggested by the gradual broadening of the peak which clearly states the better interaction between the clay and the matrix. It was also observed that the T_m of both the components changes slightly towards the lower temperature due to the fall in crystallinity.

Fig. 7 also shows two characteristic peaks in tan δ versus temperature diagram at around 65 °C and 100 °C. POE shows a sharp peak at around 100 °C. It was observed that addition of 0.5% clay did not change the peak position but broadened the peak as well as increased its height while lowers the height and sharpness of the peak of the EVA component. It corresponds to the fact that the cooperative motion of the molecules in the EVA phase is greater than that of the POE phase. Thus it may be assumed that the clay was better dispersed in the EVA phase. Again, it was observed here that storage modulus showed a decreasing trend with 0.5% clay although the tensile strength, tensile modulus and hardness showed significantly good results. The reason of this is not completely clear yet. But increased loss modulus explains the net high elongation of $E_{90/N0.5}$ instead of large crystallite thickness. High viscous part helps in better heat dissipation. It may be assumed that loss modulus dominates over the crystallite size here.

Fig. 9 and Fig. 10 represent the SEM images of the fractured surfaces of the POE/EVA blends and their corresponding nanocomposites with clay. It was observed in all the cases that the two phases were distinct and the EVA phase was dispersed in the POE matrix which in turn thus

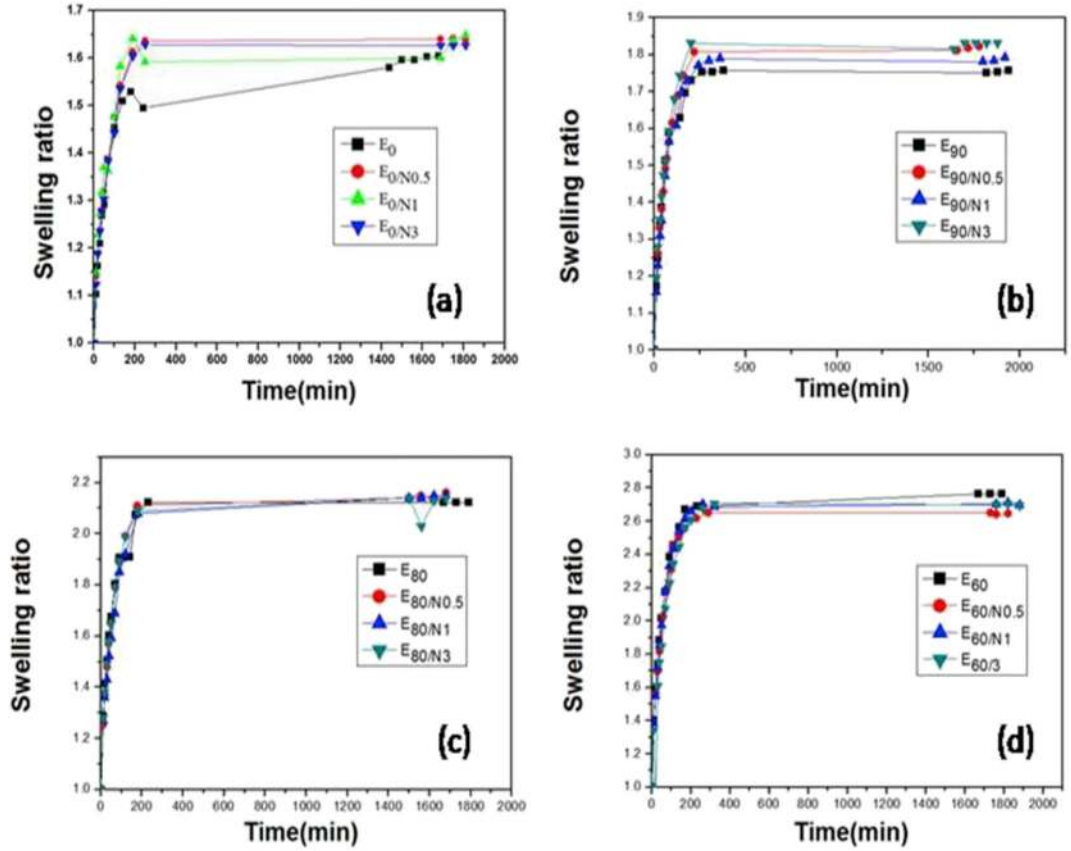

Fig. 11. Swelling studies of different composites of clay with (a) POE, (b) POE/EVA (90:10) blend, (c) POE/EVA (80:20) blend, (d) POE/EVA (60:40) blend.

Table 3
Electrical properties of all the batches.

Specimen	E_0	E_{90}	E_{80}	E_{60}	$E_{0/N0.5}$	$E_{0/N1}$	$E_{0/N3}$	$E_{90/N0.5}$	$E_{90/N1}$	$E_{90/N3}$	$E_{80/N0.5}$	$E_{80/N1}$	$E_{80/N3}$	$E_{60/N0.5}$	$E_{60/N1}$	$E_{60/N3}$
AC breakdown voltage (KV)	6	5	2	6	6	5	2	6	4	6	3	3	3	10	6	5

suggests the formation of a thermoplastic vulcanizate (TPV) through dynamic vulcanization. In Fig. 8 a. EVA of small domain sizes are distributed throughout the POE matrix. The white portions in Fig. 8 b, 8 c and 8 d represent the clay phase. It can be said from the morphology images that 0.5% clay was uniformly dispersed into the matrix along with little agglomeration thus increasing the mechanical properties also, which, 1% and 3% clay could not. Their images clearly show that the surface is fully white with 1% and 3% clay which suggests that the clay phase mainly remains on the surface. Mixing efficiency was poor in those cases.

However, Figs. 9 and 10 shows that as the EVA content was increased domain size of the dispersed phase was also increased. White lines at the interface of the EVA and POE in Fig. 9b and 9 c signify that the clay phase was mainly dispersed into the EVA phase. Addition of 3% clay caused agglomeration of the filler and thus lowered the strength. Domain size of the EVA phase is far greater than the former two batches and clay phase is more uniformly distributed around the EVA domain in Fig. 10. Thus it attributes to the fact that the polar clay phase has more affinity towards the polar EVA phase than the non polar POE matrix and thus reinforces the EVA phase mainly.

The morphological features can be further supported by Fig. 11 which demonstrates the swelling characteristics of all the batches. It was observed that EVA has greater affinity towards toluene than POE. It is noticeable that addition of EVA increases the swelling of POE which suggests the poor dispersion of the clay in POE phase and also fall in crystallinity. The interaction between the clay phase and POE is poor. In case of POE/EVA blends swelling ratio is greater than that in case of pure POE. However, as the EVA content increases the clay phase performed well in preventing the swelling. In case of E_{60} 0.5% clay even helped in decreasing the swelling to some extent. This clearly suggests that the clay phase had mainly distributed in the EVA phase. This can be further supported by the AC breakdown voltage values reported in Table 3.

It is clear that only $E_{60/N0.5}$ shows a drastic increase in the breakdown voltage value from 6 KV to 10 KV which has higher EVA content suggesting the clay phase has predominantly dispersed into the EVA phase.

4. Conclusions

It can be concluded that a new TPV/organoclay nanocomposite has been developed through dynamic vulcanization during reactive melt blending in which the clay phase is mainly distributed in the more polar component. POE/EVA TPVs reinforced with various amounts of organoclay were prepared with dicumyl peroxide as the vulcanizing agent and the clay went into the EVA phase. It was found that where E_{90} exhibited improved mechanical properties, E_{60} showed better solvent resistance properties though E_{80} also showed improvement in some of the properties upon addition of clay. However, in all the cases 0.5%

nanoclay performed well in improving those properties. The mechanical properties are highly dependent on the percent crystallinity in the nanocomposites. People have studied distribution of fillers with different dimensions in polymer blends and composites [30,31,40,41]. Similar studies can be extended in the next phase of this work whereby both dispersion and distribution of isotropic and anisotropic nanofillers can be explored.

Declaration of competing interest

The authors declare that they have no known competing financial interests or personal relationships that could have appeared to influence the work reported in this paper.

Acknowledgement

Authors are acknowledging to JK tyres, HASETRI for providing the DMA results and Leibniz Institute for Polymer Research Dresden for providing the SEM results. Authors would also like to acknowledge Dr. Arindam Giri, Dr. Abhijit Pal, Ms. Sabina Yeasmin, Ms. Tamalika Das, and Mr. Soumen Sardar (fellow research scholars) for providing technical and experimental support.

Appendix A. Supplementary data

Supplementary data to this article can be found online at https://doi.org/10.1016/j.polymertesting.2020.106374.

References

[1] Y. Kojima, A. Usuki, M. Kawasumi, A. Okada, Y. Fukushima, T. Kurauchi, O. Kamigaito, Mechanical properties of nylon 6-clay hybrid, J. Mater. Res. 8 (1993) 1185–1189, https://doi.org/10.1557/JMR.1993.1185.

[2] S.D. Burnside, E.P. Giannelis, Synthesis and properties of new poly (Dimethylsiloxane) nanocomposites, Chem. Mater. 7 (1995) 1597–1600, https://doi.org/10.1021/cm00057a001.

[3] J.W. Gilman, Flammability and thermal stability studies of polymer layered-silicate (clay) nanocomposites, Appl. Clay Sci. 15 (1999) 31–49, https://doi.org/10.1016/S0169-1317(99)00019-8.

[4] R.A. Vaia, S. Vasudevan, W. Krawiec, L.G. Scanlon, E.P. Giannelis, New polymer electrolyte nanocomposites: melt intercalation of poly(ethylene oxide) in mica-type silicates, Adv. Mater. 7 (1995) 154–156, https://doi.org/10.1002/adma.19950070210.

[5] S.S. Ray, K. Yamada, A. Ogami, M. Okamoto, K. Ueda, New polylactide/layered silicate nanocomposite: nanoscale control over multiple properties, Macromol. Rapid Commun. 23 (2002) 943–947, https://doi.org/10.1002/1521-3927(200211)23:16F.

[6] P. Liborio, V.A. Oliveira, M. de, F.V. Marques, New chemical treatment of bentonite for the preparation of polypropylene nanocomposites by melt intercalation, Appl. Clay Sci. 111 (2015) 44–49, https://doi.org/10.1016/j.clay.2015.04.003.

[7] M. Alexandre, P. Dubois, T. Sun, J.M. Garces, R. Jerome, Polyethylene-layered silicate nanocomposites prepared by the polymerization -filling technique : synthesis and mechanical properties, Polymer 43 (2002) 2123–2132, https://doi.org/10.1016/S0032-3861(02)00036-8.

[8] H. Mauroy, T.S. Plivelic, J.P. Suuronen, F.S. Hage, J.O. Fossum, K.D. Knudsen, Anisotropic clay-polystyrene nanocomposites: synthesis, characterization and mechanical properties, Appl. Clay Sci. 108 (2015) 19–27, https://doi.org/10.1016/j.clay.2015.01.034.

[9] J.W. Cho, D.R. Paul, Nylon 6 nanocomposites by melt compounding, Polymer (Guildf) 42 (2001) 1083–1094, https://doi.org/10.1016/S0032-3861(00)00380-3.

[10] Z. Wang, T.J. Pinnavaia, Hybrid organic-inorganic nanocomposites: exfoliation of magadiite nanolayers in an elastomeric epoxy polymer, Chem. Mater. 10 (1998) 1820–1826, https://doi.org/10.1021/cm970784o.

[11] S. Varghese, J. Karger-Kocsis, Natural rubber-based nanocomposites by latex compounding with layered silicates, Polymer (Guildf) 44 (2003) 4921–4927, https://doi.org/10.1016/S0032-3861(03)00480-4.

[12] M. Pramanik, S.K. Srivastava, B.K. Samantaray, A.K. Bhowmick, EVA/Clay nanocomposite by solution blending: effect of aluminosilicate layers on mechanical and thermal properties, Macromol. Res. 11 (2003) 260–266, https://doi.org/10.1007/BF03218362.

[13] S. Mondal, A. Das, J. Bandyopadhyay, S.S. Ray, G. Heinrich, A. Bandyopadhyay, A noble additive cum compatibilizer for dispersion of nanoclay into ethylene octene elastomer, Appl. Clay Sci. 126 (2016) 41–49, https://doi.org/10.1016/j.clay.2016.02.032.

[14] M. Siliani, M.A. López-Manchado, J.L. Valentín, M. Arroyo, A. Marcos, M. Khayet, J.P.G. Villaluenga, Millable polyurethane/organoclay nanocomposites: preparation, characterization, and properties, J. Nanosci. Nanotechnol. 7 (2007) 634–640, https://doi.org/10.1166/jnn.2007.134.

[15] Y.W. Chang, Y. Yang, S. Ryu, C. Nah, Preparation and properties of EPDM/organomontmorillonite hybrid nanocomposites, Polym. Int. 51 (2002) 319–324, https://doi.org/10.1002/pi.831.

[16] S. Sadhu, A.K. Bhowmick, Preparation and properties of styrene-butadiene rubber based nanocomposites: the influence of the structural and processing parameters, J. Appl. Polym. Sci. 92 (2004) 698–709, https://doi.org/10.1002/app.13673.

[17] S. Sadhu, A.K. Bhowmick, Preparation and properties of nanocomposites based on acrylonitrile- butadiene rubber, styrene-butadiene rubber, and polybutadiene rubber, J. Polym. Sci., Part B: Polym. Phys. 42 (2004) 1573–1585, https://doi.org/10.1002/polb.20036.

[18] M. Huskić, A. Anžlovar, M. Žigon, Montmorillonite-phenolic resin nanocomposites prepared by one-step in-situ intercalative polymerisation, Appl. Clay Sci. 101 (2014) 484–489, https://doi.org/10.1016/j.clay.2014.09.011.

[19] A. Gu, S.W. Kuo, F.C. Chang, Syntheses and properties of PI/clay hybrids, J. Appl. Polym. Sci. 79 (2001) 1902–1910, https://doi.org/10.1002/1097-4628(20010307)79:10<1902::AID-APP190>3.0.CO;2-S.

[20] K. Kowalczyk, T. Spychaj, A. Ubowska, B. Schmidt, Industrially applicable methods of poly(methyl methacrylate)/organophilic montmorillonite nanocomposites preparation: processes and cast materials characterization, 97–98, Appl. Clay Sci. (2014) 96–103, https://doi.org/10.1016/j.clay.2014.05.011.

[21] D. Lee, S.H. Lee, K. Char, J. Kim, Expansion distribution of basal spacing of the silicate layers in polyaniline/Na+-montmorillonite nanocomposites monitored with X-ray diffraction, Macromol. Rapid Commun. 21 (2000) 1136–1139, https://doi.org/10.1002/1521-3927(20001101)21:16<1136::AID-MARC1136>3.0.CO;2-S.

[22] A.K. Bhowmick, T. Inoue, Structure development during dynamic vulcanization of hydrogenated nitrile rubber/nylon blends, J. Appl. Polym. Sci. 49 (1993) 1893–1900, https://doi.org/10.1002/app.1993.070491104.

[23] M.H.R. Ghoreishy, M. Razavi-Nouri, G. Naderi, Finite element analysis of a thermoplastic elastomer melt flow in the metering region of a single screw extruder, Comput. Mater. Sci. 34 (2005) 389–396, https://doi.org/10.1016/j.commatsci.2005.01.011.

[24] A. M Gessler, Cranford, W.H. Haslett, Process for Preparing a Vulcanized Blend of Crystalline Polypropelene and Chlorinated Butyl Rubber, Us papent, 1962.

[25] P.E.J. Seccuro, United States patent, Geothermics 14 (1985) 595–599, https://doi.org/10.1016/0375-6505(85)90011-2.

[26] P.E.C. Bleutge, United States patent, Geothermics 14 (1985) 595–599, https://doi.org/10.1016/0375-6505(85)90011-2.

[27] Y. Tsai, J.H. Wu, Y.T. Wu, C.H. Li, M.T. Leu, Reinforcement of dynamically vulcanized EPDM/PP elastomers using organoclay fillers, Sci. Technol. Adv. Mater. 9 (2008), https://doi.org/10.1088/1468-6996/9/4/045005.

[28] S. Kole, D.K. Tripathy, Morphology and ageing behaviour of silicone-EPDM blends, J. Mater. Sci. 29 (1994) 2431–2435, https://doi.org/10.1007/BF00363437.

[29] X. Liu, H. Huang, Z. Xie, Y. Zhang, Y. Zhang, K. Sun, L. Min, EPDM_polyamide TPV Compatibilized by chlorinated.Pdf, vol. 22, 2003, pp. 9–16.

[30] J. Huang, L. Cao, D. Yuan, Y. Chen, Design of novel self-healing thermoplastic vulcanizates utilizing thermal/magnetic/light-triggered shape memory effects, ACS Appl. Mater. Interfaces 10 (2018) 40996–41002, https://doi.org/10.1021/acsami.8b18212.

[31] J. Huang, L. Cao, D. Yuan, Y. Chen, Design of multi-stimuli-responsive shape memory biobased PLA/ENR/Fe3O4 TPVs with balanced stiffness-toughness based on selective distribution of Fe3O4, ACS Sustain. Chem. Eng. 7 (2019) 2304–2315, https://doi.org/10.1021/acssuschemeng.8b05025.

[32] H.H. Le, K. Oßwald, S. Wießner, A. Das, K.W. Stöckelhuber, R. Boldt, G. Gupta, G. Heinrich, H.J. Radusch, Location of dispersing agent in rubber nanocomposites during mixing process, Polymer (Guildf). 54 (2013) 7009–7021, https://doi.org/10.1016/j.polymer.2013.10.038.

[33] A. Biswas, A. Bandyopadhyay, N.K. Singha, A.K. Bhowmick, Chemical modification of metallocene-based polyethylene–octene elastomer through solution grafting of acrylic acid and its effect on the physico-mechanical properties, J. Appl. Polym. Sci. 105 (2007) 3409–3417, https://doi.org/10.1002/app.26374.

[34] A. Biswas, A. Bandyopadhyay, N.K. Singha, A.K. Bhowmick, Ionomeric modification of a metallocene-based polyolefinic elastomer and its influence on the physicomechanical properties: effects of the crystallinity and pendent chain length, J. Appl. Polym. Sci. 114 (2009) 3906–3914, https://doi.org/10.1002/app.30662.

[35] A. Biswas, A. Bandyopadhyay, N.K. Singha, A.K. Bhowmick, Sulfonation of metallocene-based polyolefinic elastomers and its influence on physicomechanical properties: effect of reaction parameters, styrene grafting, and pendant chain length, J. Polym. Sci., Part A: Polym. Chem. 46 (2008) 8023–8040, https://doi.org/10.1002/pola.23101.

[36] K. Naskar, S. Mohanty, G.B. Nando, Development of thin-walled halogen-free cable insulation and halogen-free fire-resistant low-smoke cable-sheathing compounds based on polyolefin elastomer and ethylene vinyl acetate blends, J. Appl. Polym. Sci. 104 (2007) 2839–2848, https://doi.org/10.1002/app.25870.

[37] R. Pervin, L. Goswami, V. Vijayabaskar, A. Bandyopadhyay, Optimization of engineering and solvent resistive behavior of high vinyl acetate content EVA-modified poly(ethylene-*co*-1-octene) interpenetrating network blends using taguchi orthogonal array, J. Appl. Polym. Sci. 126 (2012) 1993–2003, https://doi.org/10.1002/app.36684.

[38] H.J. Tai, Random crosslinking of an ethylene vinyl acetate copolymer and a metallocene polyolefin elastomer in the presence of polyfunctional monomers, Polymer (Guildf) 42 (2001) 5207–5213, https://doi.org/10.1016/S0032-3861(01)00003-9.

[39] M. Tokihisa, K. Yakemoto, T. Sakai, L.A. Utracki, M. Sepehr, J. Li, Y. Simard, Extensional flow mixer for polymer nanocomposites, Polym. Eng. Sci. 46 (2006) 1040–1050, https://doi.org/10.1002/pen.20542.
[40] J. Huang, J. Fan, S. Yin, Y. Chen, Y, Design of remotely, locally triggered shape-memory materials based on bicontinuous polylactide/epoxidized natural rubber thermoplastic vulcanizates via regulating the distribution of ferroferric oxide, Compos. Sci. Technol. 182 (2019) 107732, https://doi.org/10.1016/j.compscitech.2019.107732.
[41] Y. Liu, L. Cao, D. Yuan, Y. Chen, Design of super-tough co-continuous PLA/NR/SiO2 TPVs with balanced stiffness-toughness based on reinforced rubber and interfacial compatibilization, Compos. Sci. Technol. 165 (2018) 231–239, https://doi.org/10.1016/j.compscitech.2018.07.005.